Research Article

Computational evaluation of altered biomechanics related to articular cartilage lesions observed *in vivo*†

Katariina A. H. Myller[1,2,3], Rami K. Korhonen[1,2], Juha Töyräs[1,2,7], Jari Salo[5,6], Jukka S. Jurvelin[1,2], Mikko S. Venäläinen[1,4]

[1] Department of Applied Physics, University of Eastern Finland, Kuopio, Finland

[2] Diagnostic Imaging Center, Kuopio University Hospital, Kuopio, Finland

[3] Centre of Oncology, Kuopio University Hospital, Kuopio Finland

[4] Turku Centre for Biotechnology, University of Turku and Åbo Akademi University, Turku, Finland

[5] Orthopaedics and Traumatology Clinic, Mehiläinen, Helsinki, Finland

[6] Department of Orthopaedics, Traumatology and Hand Surgery, Kuopio University Hospital, Kuopio, Finland

[7] School of Information Technology and Electrical Engineering, The University of Queensland, Brisbane, Australia

Correspondence:

Katariina AH Myller, MSc.

Department of Applied Physics, University of Eastern Finland

P.O. Box 1627, 70211 Kuopio, Finland

Tel: +358 504659802

Fax: +358 162585

Email: katariina.myller@uef.fi

†This article has been accepted for publication and undergone full peer review but has not been through the copyediting, typesetting, pagination and proofreading process, which may lead to differences between this version and the Version of Record. Please cite this article as doi: [10.1002/jor.24273]

Received 24 September 2018; Revised 19 Janaury 2019; Accepted 17 February 2019

Journal of Orthopaedic Research®

DOI 10.1002/jor.24273

Email addresses of co-authors: rami.korhonen@uef.fi, juha.toyras@uef.fi, jari.salo@mehilainen.fi, jukka.jurvelin@uef.fi, mikko.venalainen@utu.fi

Manuscript length 3716 words (the main text), 6 figures, 1 table

ABSTRACT

Chondral lesions provide a potential risk factor for development of osteoarthritis. Despite the variety of *in vitro* studies on lesion degeneration, *in vivo* studies that evaluate relation between lesion characteristics and the risk for the possible progression of OA are lacking. Here, we aimed to characterize different lesions and quantify biomechanical responses experienced by surrounding cartilage tissue. We generated computational knee joint models with nine chondral injuries based on clinical *in vivo* arthrographic computed tomography images. Finite element models with fibril-reinforced poro(visco)elastic cartilage and menisci were constructed to simulate physiological loading. Systematically, the lesions experienced increased maximum principal and maximum shear strains and, moreover, decreased minimum principal strain in the surrounding chondral tissue (p<0.01) compared with intact tissue. Depth, volume and area of the lesion correlated with the maximum shear strain (p<0.05, Spearman rank correlation coefficient ρ=0.733-0.917). Depth and volume of the lesion correlated also with the maximum principal strain (p<0.05, ρ=0.767 and ρ=0.717, respectively). However, the lesion area had non-significant correlation with this strain parameter (p=0.06, ρ=0.65). Potentially, the introduced approach could be developed for clinical evaluation of biomechanical risks of a chondral lesion and planning an intervention.

Statement of Clinical Relevance: In this study, we computationally characterized different *in vivo* chondral lesions and evaluated their risk of cartilage degeneration. This information is vital in decision-making for intervention in order to prevent post-traumatic osteoarthritis.

Key terms: Knee joint, Injury, Computed tomography, Osteoarthritis, Finite element analysis

INTRODUCTION

Chondral lesions might be caused by injury or trauma, possibly leading to degeneration of articular cartilage and post-traumatic osteoarthritis (OA)[1–3]. OA is a common joint disease, with irreversible nature, causing pain and immobility[4]. The degeneration mechanisms in articular cartilage are complicated and comprise several factors from the abnormal joint structure to inflammation processes[5–7]. Inevitably, biomechanics of the joint and loading of the tissue contribute to the degeneration process[7–11]. Nevertheless, no clear consensus exists on which kind of lesions result in OA and which characteristics might be the most contributory related to further degeneration.

Novel imaging techniques and sophisticated computational modeling offer new insights in the evaluation of injuries in the knee joint and to examine the joint function. Arthrographic computed tomography (CT) utilizes contrast agents which enable rapid visualization of cartilage defects in high resolution[12,13]. Despite the invasiveness of the contrast agent injection, in professional use they are considered safe[14–16]. Furthermore, the arthrographic CT allows for quantifying spatial distribution of subchondral bone mineral density[17,18]. Based on imaging data, finite element (FE) modeling can be further applied to simulate the biomechanical function of the knee under physiologically relevant loading conditions[19–22]. Simulation of knee joint function can reveal diagnostically valuable information on the status of the joint; for instance, strain or stress levels and distributions in the cartilage can be applied to estimate the failure of the tissue[19,23–25]. At present, this kind of quantitative

evaluation of the biomechanical response of the tissue is unachievable without computational modeling.

A recent study combined arthrographic CT imaging with FE modeling to study the biomechanical response of tibial cartilage around a chondral lesion during walking[20]. It was observed that even though the presence of cartilage defects increases the experienced strains in tissue adjacent to a lesion, the amplitude of changes is highly dependent on the location of the lesion on the articular surface. However, this study investigated the alterations only in a single knee. Additionally, in another computational study with simplified loading, it was observed that both larger lesion size and high weight-bearing location are factors potentially contributory to OA progression[26]. However, since cartilage lesions can be found on all articulating surfaces of the knee and they can considerably vary in both shape and size, more investigations with physiologically relevant loading conditions and different knee joint geometries are needed to better understand the role of lesion characteristics in biomechanical response of the tissue in a patient-specific manner. In clinical decision making, treatment and rehabilitation are highly dependent on the information about the lesion severity[6,27].

The aim of this study was to examine the effect of chondral lesions on the biomechanical response of knee joint cartilage using clinical arthrographic CT imaging and FE modeling. The detailed geometries of the knee joints with cartilage lesions were obtained from the arthrographic CT images to create FE representations of the joint with advanced tissue-specific material properties. In all cases, the knee joint function was simulated under loading conditions mimicking the stance phase of gait. Here, we focused on analyzing the effect of the characteristics of the lesion on the tensile, shear, and compressive strains in the surrounding tissue since they have been linked to cartilage matrix damage or chondrocyte apoptosis in previous experimental studies[28–30]. We hypothesized that combining arthrographic CT imaging with FE modeling could reveal novel insights into the contribution of

different lesion characteristics to alterations in cartilage biomechanics as well as enable the classification of lesions into higher and lower risk subgroups.

METHODS

Patients

Five subjects with possible knee joint injuries were enrolled in the study after giving a written consent and having a clinical examination. The study protocol was reviewed by the Ethical Committee of Kuopio University Hospital, Kuopio, Finland (Favourable Opinion No: 54/2011) and the study adhered the Declaration of Helsinki.

Imaging and segmentation

Knees (n = 5) of the patients were imaged using cone beam computed tomography (CBCT) device (Verity, Planmed Oy, Finland). The patients were in a sitting position during imaging. Prior to imaging, an anionic contrast agent (V = 20 mL, q = −1, M = 1269 g/mol, 320 mg iodine/ml, Hexabrix™, Mallinckrodt Inc., St. Louis, MO, USA), diluted to half of its concentration using saline, was injected into the joint space. Subsequently, the knee joint was flexed and extended a couple of times to ensure even distribution of the contrast agent. During the CT imaging, patients had a custom-made hydroxyapatite phantom belt placed around the tibia[17]. Tube voltage of 100 kV and 54 mAs were used with a voxel size of 200 x 200 x 200 μm^3. In total, nine distinct defects were observed in the imaged knee joints. Segmentation of articular cartilages, menisci, bones, and lesions was done manually using an open source software (Fig. 1 a) (v2.2.3, Seg3D, Scientific Computing and Imaging Institute, University of Utah, UT, USA). Geometries of lesion sites with intact tissue were also created; the geometry was otherwise exactly the same, but the cartilage surface was considered as

intact. In addition to segmentation of damaged cartilage, masks representing completely intact tissue were also created by manually interpolating the intact tissue surface over the defect, similarly as before[20] .

In order to analyze the detailed biomechanical response of the chondral lesion with minimum computational cost, submodeling approach was applied to all lesion sites to allow for a greater mesh density within the region of interest[20] (Fig. 1 b). This approach allowed us to observe the subtle alterations in strain patterns in the defected cartilage site (Fig. 1 c).

Finite element analysis

Segmentations were first converted to 3D stereolithographic (STL) format for post-processing in an open source mesh processing software (MeshLab, ISTI – CNR, www.meshlab.net). After minimizing the amount of surface irregularities and decreasing the number of tiny surface elements, the surface meshes were converted into Standard ACIS Text (SAT) format (MATLAB, R2014a, MathWorks Inc., Natick, MA, USA) for the modelling. Abaqus (v6.14, Dassault Systèmes, Providence, RI, USA) was used for the generation of the finite element models and running the simulations.

Linear, hexahedral elements (type C3D8P) were used for all tissues except for bone which was meshed using first order tetrahedral elements (type C3D4). In the lesion region, second order tetrahedral elements (type C3D10P) were applied to cartilage to retain realistic shape of the lesion. On average, element sizes of ~2.9 mm, ~2.3 mm, ~2.4 mm, and ~1.8 mm were used for bone, femoral cartilage, tibial cartilage and menisci in the joint-level analysis, respectively. The surface area of the lesion was defined as an area between the edges of the lesion. It was determined by summing up of the area of the faces from the corresponding area in the generated intact surface mesh.

Fibril-reinforced poroviscoelastic (FRPVE) and fibril-reinforced poroelastic (FRPE) material properties were applied for cartilage and menisci, respectively. In principle, the FRPVE material is composed of porohyperelastic non-fibrillar matrix, to represent the mechanical function of tissue proteoglycans and interstitial fluid, and viscoelastic fibrillar matrix to represent the function of collagen fibrils[31,32]. In the FRPE material, collagen fibrils were assumed elastic. In cartilage, the primary collagen fibrils followed an arcade-like depth-wise orientation, aligning into distinct split-line patterns on the articular surface (Fig. 1 a)[31–34] whereas in menisci, the primary collagen fibrils were oriented circumferentially[35]. The present values of material parameters have been previously reported for both cartilage[19] and menisci[36]. Similarly as before, the material properties implemented for the damaged cartilage were the same as for the intact tissue at the same location and no alterations in the fibrillar or non-fibrillar matrix were considered[20]. The attachments of meniscal horns to the tibia were modeled using linear springs with total spring constants of 350 N/mm[37]. These springs resisted only tension.

Bone was modelled as linearly elastic and isotropic material with element-specific Young's modulus based on CT Hounsfield units (HU) (Fig. 1 a). Correspondence between HU values and bone mineral density was defined using the custom-made hydroxyapatite phantoms with their known volumetric bone mineral densities[17]. The conversion of bone mineral densities to Young's moduli was made using density-elasticity relationship and assigned to each element using an advanced mapping strategy[38,39], similarly as in the previous study[18].

In all cases, the function of the knee was simulated under loading conditions typical to the stance phase of gait. Since subject-specific information on kinematics and kinetics of walking was not available, the loading protocol was obtained from the literature. This was implemented by applying the time-dependent axial force, scaled based on subject's weight, and flexion angle[40,41] (Fig. 1 a) to the reference point located at the middle of transepicondylar axis of femur and fixing the distal end

of tibia. Varus-valgus movement was set free to ensure sufficient contact between both lateral and medial condyles of the knee[19,42] whereas anterior-posterior and medial-lateral movements were restricted due to their small variations and internal-external rotation due to its patient-specific alteration[43,44]. More detailed description of implementing the load can be found from the previous study[20].

All mechanical contacts between articulating surfaces and menisci were assumed to be frictionless[45] and were modeled using pressure-overclosure relationship and surface-to-surface discretization. Since the loading in the model is instantaneous, cartilage can be considered incompressible and fluid flow through surfaces can be considered negligible[36], and, therefore, it was restricted through all articular cartilage and meniscus surfaces except on the inner boundaries of the defect. This reflects fluid flow through the defect surfaces due to collagen damage and the effect of missing intact superficial collagen fibril network that contributes to fluid pressure[46].

In order to decrease the calculation time and enable subtle analysis of the defects, submodels (Fig. 1 b) with substantially denser meshes were created for the chondral lesion sites for both damaged and intact cartilage. In all submodels, at least 3 mm wide zone of intact cartilage tissue was included in the region of interest around the defect. The displacements of the exterior surfaces of region of interest in the global model were used to drive the mechanical response of the submodel. All submodels were meshed using linear tetrahedral elements (type C3D4P). This element type was previously observed to restrict excessive element distortion efficiently leading to convergence difficulties[20]. The average element size in the submodels was ~0.7 mm and the sufficiency of the mesh densities was verified by carrying out additional simulations with denser meshes. A mesh density was considered to be sufficient if absolute differences of less than 2% were observed in the peak values of studied strain measures between the selected mesh and a denser mesh.

Comparison of lesions and statistical analysis

The effect of the lesion on the biomechanical response of surrounding cartilage was evaluated in terms of changes in maximum principal (tensile) strain, minimum principal (compressive) strain and shear strain, of the tissue by comparing defect and intact (artificially corrected lesion) sites. These parameters were chosen since they have been linked to the failure of the cartilage tissue[28,47]. The peak values of these variables during gait were determined within the 1 mm distance from the lesion and compared using the Wilcoxon signed rank test (R, v3.4.2, R Core Team[48]). Spearman rank correlation was used for the comparison of lesion properties with changes in different strain measures. The parameters characterizing the lesions included maximum lesion depth (normalized with respect to the thickness of healthy tissue), surface area of the lesion, and volume of the lesion. In addition, to estimate the relative stress level at the lesion site, average cumulative stress during the whole gait was calculated similarly as in a previous study[19] and normalized using the maximum cumulative stress in the joint compartment.

RESULTS

FE models of knee joints (n = 5) with chondral lesions (nine in total) were constructed based on 3D geometries generated from arthrographic CT image segmentations (Fig. 1). In all five knee joints, cartilage defect observed in the medial femoral condyle was found to alter the strain distributions in the tissue surrounding the defect (Fig. 2). Although the amplitude and extent of changes varied greatly between different lesions, maximum principal strains were typically elevated close to lesion edges as compared to the intact tissue. Similar changes were also observed for lesions located on other articulating surfaces of the knee (Fig. 3). However, the magnitude and extent of changes varied between different lesions.

Despite different shapes, sizes and locations of the lesions, statistically significant increases in peak values of maximum principal strains and maximum shear strains ($p < 0.01$, Wilcoxon signed rank test) were observed in the tissue within 1 mm distance from the defect between the models with damaged and intact cartilage (Fig. 4). Similarly, a statistically significant decrease in peak values of minimum principal strains ($p < 0.01$) was found. In median values of peak maximum principal strains and shear strains, the increases were approximately 1.6-fold and 2.0-fold, respectively, whereas in median minimum principal strains, the decrease was approximately 1.6-fold. For only the lesions of the medial femoral condyle, the differences were nearly significant ($p = 0.06$).

The correspondence between changes in peak strain values (maximum principal strain, minimum principal strain, and shear strain) and lesion size parameters (depth, area, and volume) was calculated (Table 1). A very high positive correlation (Spearman rank correlation coefficient $\rho = 0.917$, $p < 0.01$) was found between the lesion depth and maximum shear strain. Furthermore, a good correlation was found when comparing depth and volume of the lesion with the maximum principal strain. The average cumulative stress distribution on the knee was calculated during the gait to determine the level of the cumulative stress at the lesion sites. This was done to study the effect of the chondral lesion location, *i.e.* relative stress level, in the knee. Despite of varying shape and size, most of the lesions were located at areas under high cumulative stress over one loading cycle (Fig. 5). A strong dependence ($\rho = 0.883$ - 0.933, $p < 0.01$) was found between the relative stress level and all of the size parameters (depth, area, and volume).

DISCUSSION

In this study, the effect of different chondral lesions, observed in a clinical *in vivo* setting, on the biomechanical response of articular cartilage in human knee was evaluated. The changes in the biomechanical response, as compared to healthy tissue, were studied in terms of changes in maximum

principal (tensile) strains, minimum principal (compressive) strains and shear strains. In addition, the association of changes to the fundamental characteristics of the lesion, *i.e.* depth, area, volume and location, was evaluated.

All the lesions caused noticeable changes in the studied strain measures in the tissue surrounding the defect (Fig. 4). This is most probably related to inconsistent geometries of lesions; the decrease in the cartilage-cartilage contact area due to discontinuity and irregularity of cartilage surface might be the reasons why, for example, the edges of lesions experience higher maximum principal strains (Fig. 2, Fig. 3). Noticeably, the median levels of minimum principal strains and shear strains were also found to reach levels corresponding to previously suggested failure limits for cartilage, *i.e.* -30% and 32%, respectively[28,47]. Naturally, bottoms of the lesions, which lack the direct contact with the opposing articulating surface, experienced lower maximum principal strains. Since higher strains predispose the tissue for deterioration either via failure of the collagen network or cell apoptosis[28,30,47], our results suggest that the presence of lesions can increase the risk of tissue degeneration. However, the change in strains was found to vary greatly and the suggested failure limits were exceeded only in some of the lesions. Notably, all the lesions exceeding the failure limit for shear strain exceeded also the failure limit for minimum principal strain.

The lesion depth had high correlation with changes in both maximum principal strain and shear strain whereas the area had slightly less effect on the strains. This contradicts slightly with the current cartilage lesion diagnostics from magnetic resonance images (MRI) that trust evaluation of the area of the lesion[49]. Moreover, MRI has been reported to have challenges in accurate detection of shape and size of chondral lesions[50].

The distribution of the lesion locations did not cover the joint surface; most of the lesions were located at areas with high cumulative stress (Fig. 5). Interestingly, in curved lesions, the inner and shorter side showed higher stresses than the longer outer border. This could suggest that in cartilage repair

procedures special attention should be paid to clean this side to form more round-like than flap-like area on the cartilage surface. Potentially, this kind of repairing procedure could help to decrease the shear strains and inhibit further damage of the cartilage. Altogether, our suggested approach enables dividing lesions into higher and lower risk ones based on their strain levels which can help to make the decision of the intervention.

Maximum shear strains correlated to all the lesion size parameters (Table 1). Higher values in shear strain at area close to a lesion are conceivably due to the material properties of cartilage; the uppermost layer of the cartilage consists of collagen network which is parallel to the surface[34] (Fig. 1 a), therefore restricting excessive shear strains. When the uppermost surface of the cartilage is lacking, the surface movements parallel to the surface are freer.

Interestingly, none of the lesion properties correlated statistically significantly with minimum principal strain, possibly indicating that compression of the cartilage tissue around the lesion is more non-systematic. On the other hand, the size of the lesion correlated with its location on the joint: the higher the cumulative stresses on the lesion region, the greater the lesion. This is in line with the previous studies, *i.e.* the location of the lesion is usually at the medial condyle[51], known as the contact area in the joint where the stresses are higher.

Previously, the prevalence and progression of chondral lesions as well as alterations in cartilage biomechanics in *in vitro* models of cartilage lesions have been investigated[52–59]. *In vitro* models and strain-based degeneration algorithm have, for example, been able to reproduce experimentally found cartilage degeneration in terms of proteoglycan loss under similar levels of strain as reported here[60,61]. In spite of these investigations, no other studies exist, to the best of our knowledge, which have studied the relationship between simulated articular cartilage biomechanics and lesion characteristics using *in vivo* data from several clinically observed cartilage lesions. Our results point out relevant aspects to be taken into account when considering an intervention; this kind of quantitative approach

could be clinically used for classifying lesions as higher or lower risk for the progression of OA. Even though the longitudinal analysis of lesion progression was not possible to carry out in the current study due to absence of follow-up data, the present findings serve as an important next step towards understanding the changes in the biomechanics of the knee due to cartilage lesions.

Previous studies have shown that articular cartilage properties, such as proteoglycan content at areas close to lesion, differ from the other cartilage tissue in the joint[58], possibly indicating post-traumatic degeneration of cartilage. Depletion of proteoglycans have been suggested to be one of the earliest signs in OA development and, further, disruption of the collagen network occurs in OA[62]. Here, the effect of changes in material properties of cartilage were not modeled because we assumed that tissue properties do not change immediately after injury. Nevertheless, it has been reported previously that both the disruption of the collagen network and the loss of proteoglycan content can lead to increased strains in cartilage[63,64] and that the increased strains can further contribute to the progressive loss of tissue integrity and function in an iterative manner[21,65]. Therefore, it is expected that the inclusion of changes in cartilage structure and composition would have only emphasized the effect of cartilage lesions in the present study. Previously, spatial differences in material properties, such as subject-specific collagen architecture and fixed charge density distributions, have been estimated and implemented in FE models of the knee using T2 mapped[66] or ^{23}Na MR imaging[67], respectively. Since diffusion of contrast agents in contrast-enhanced CT imaging has been found to correlate with proteoglycan content[68–70], CBCT arthrography has potential to acquire lesion-specific tissue properties for modeling purposes. In addition to measuring strain values, stress-based failure criteria have been used in evaluation of cartilage degeneration around lesions[20]. However, since maximum principal stresses in cartilage have been suggested to be connected to degeneration caused by chronic overloading[19,71], we prioritized our analyses to the strain measures that have experimentally shown to be related to tissue degeneration, *i.e.* cell death or proteoglycan loss, close to lesions[21,60,61].

We aimed to analyze real lesions, instead of artificially created ones, at their actual locations, *i.e.* at both tibial and femoral cartilage and at different distances from the contact area. To make assessments reliable, we analyzed lesions by calculating the difference of defected and intact surface from the same region. This study concentrates on the biomechanical aspects of the lesion using patient-specific geometries from *in vivo* arthrographic CT data and general gait simulation. The literature-based loading resulted in contact pressures that agreed well with previously reported contact pressures. For example, during the first peak load of the stance phase, the peak contact pressures on the studied articulating surfaces varied between 7 MPa and 11 MPa which is within the range of 2-15 MPa reported in a number of experimental[72–74] and numerical studies[20,42,75,76]. Furthermore, for almost all of the models with intact cartilage, the peak compressive strains (Fig. 4b) were within the 7-23% range reported for cartilage in the tibiofemoral contact[77]. Minor differences between the model predictions and values reported in the literature are most likely due to individual variation and differences in loading conditions. Overall, these findings suggest that our model predictions represented realistic measures of knee and contact biomechanics during the stance phase of gait.

To our best knowledge, this is the first study to computationally characterize the biomechanical response of different focal chondral lesions observed in a clinical, *in vivo* set. All the lesions caused changes in the strain levels of the surrounding cartilage, indicating elevated risk for the degeneration. However, substantial variation in these changes was observed between the lesions. The depth and volume of the lesion within the joint were found to be the main factors affecting strains in the cartilage tissue. This indicates that more than one characteristic should be taken in consideration when evaluating severity of lesions, and when planning an intervention. Potentially, this study introduces a novel approach to develop quantitative and multivariate analysis method to predict mechanical risk of the lesion.

ACKNOWLEDGEMENTS

The research leading to these results has received funding from Academy of Finland (307932, and 269315), the Research Committee of the Kuopio University Hospital Catchment Area for the State Research Funding (project 5041757), Kuopio, Finland), and Doctoral Program in Science, Technology, and Computing (SCITECO, University of Eastern Finland). CSC—IT Center for Science, Finland, is acknowledged for providing computational resources and the modeling software.

AUTHOR CONTRIBUTIONS

K.A.H.M.: design of the study, conducting analyses, interpreting the results, the main writer of the manuscript, approval of the manuscript; R.K.K.: design of the study, interpreting the results, critical review of the manuscript, approval of the manuscript; J.T.: design of the study, interpreting the results, critical review of the manuscript, approval of the manuscript, J.S.: design of the study, interpreting the results, critical review of the manuscript, approval of the manuscript; J.S.J.: design of the study, interpreting the results, critical review of the manuscript, approval of the manuscript; M.S.V.: original design of the study, running simulations, conducting analyses, interpreting the results, writing the manuscript, approval of the manuscript.

COMPETING INTERESTS

The authors declare no conflicts of interest.

REFERENCES

1. Gelber AC, Hochberg MC, Mead LA, et al. 2000. Joint Injury in Young Adults and Risk for Subsequent Knee and Hip Osteoarthritis. Ann. Intern. Med. 133(5):321–328.

2. Wang Y, Ding C, Wluka AE, et al. 2006. Factors affecting progression of knee cartilage defects in normal subjects over 2 years. Rheumatology 45(1):79–84.

3. Niu J, Felson DT, Neogi T, et al. 2015. Patterns of coexisting lesions detected on magnetic resonance imaging and relationship to incident knee osteoarthritis: The multicenter osteoarthritis study. Arthritis Rheumatol. 67(12):3158–3165.

4. Arden N, Nevitt MC. 2006. Osteoarthritis: Epidemiology. Best Pract. Res. Clin. Rheumatol. 20(1):3–25.

5. Katagiri H, Mendes LF, Luyten FP. 2017. Definition of a Critical Size Osteochondral Knee Defect and its Negative Effect on the Surrounding Articular Cartilage in the Rat. Osteoarthr. Cartil. 25(9):1531–1540.

6. Anderson DD, Chubinskaya S, Guilak F, et al. 2011. Post-traumatic osteoarthritis: Improved understanding and opportunities for early intervention. J. Orthop. Res. 29(6):802–809.

7. Guilak F, Fermor B, Keefe FJ, et al. 2004. The Role of Biomechanics and Inflammation in Cartilage Injury and Repair. Clin. Orthop. Relat. Res. 423(423):17–26.

8. Henao-Murillo L, Ito K, van Donkelaar CC. 2018. Collagen Damage Location in Articular Cartilage Differs if Damage is Caused by Excessive Loading Magnitude or Rate. Ann. Biomed. Eng. 46(4):1–11.

9. Miller RH, Edwards WB, Brandon SCE, et al. 2014. Why Don't Most Runners Get Knee Osteoarthritis? A Case for Per-Unit-Distance Loads. Med. Sci. Sport. Exerc. 46(3):572–579.

10. Sadeghi H, Shepherd DET, Espino DM. 2018. Effect of the variation of loading frequency on surface failure of bovine articular cartilage. Osteoarthr. Cartil. 23(12):2252–2258.

11. Saxby DJJ, Lloyd DGG. 2017. Osteoarthritis year in review 2016: mechanics.

12. Kokkonen HT, Suomalainen J, Joukainen A, et al. 2014. In vivo diagnostics of human knee cartilage lesions using delayed CBCT arthrography. J. Orthop. Res. 32(3):403–12.

13. Myller KAH, Turunen MJ, Honkanen JTJ, et al. 2017. In Vivo Contrast-Enhanced Cone Beam CT Provides Quantitative Information on Articular Cartilage and Subchondral Bone. Ann. Biomed. Eng. 45(3):811–818.

14. Buijs SB, Barentsz MW, Smits MLJ, et al. 2017. Systematic review of the safety and efficacy of contrast injection via venous catheters for contrast-enhanced computed tomography. Eur. J. Radiol. Open 4:118–122.

15. Macht S, Beseoglu K, Eicker S, et al. 2012. Safety and feasibility in highly concentrated contrast material power injections for CT-perfusion studies of the brain using central venous catheters. Eur. J. Radiol. 81(8):1883–1885.

16. Lenhard DC, Pietsch H, Sieber MA, et al. 2012. The Osmolality of Nonionic, Iodinated Contrast Agents as an Important Factor for Renal Safety. Invest. Radiol. 47(9):503–510.

17. Turunen MJ, Töyräs J, Kokkonen HT, Jurvelin JS. 2015. Quantitative Evaluation of Knee Subchondral Bone Mineral Density Using Cone Beam Computed Tomography. IEEE Trans. Med. Imaging 34(10):2186–2190.

18. Venäläinen MS, Mononen ME, Salo J, et al. 2016. Quantitative Evaluation of the Mechanical Risks Caused by Focal Cartilage Defects in the Knee. Sci. Rep. 6:37538.

19. Mononen ME, Tanska P, Isaksson H, Korhonen RK. 2016. A Novel Method to Simulate the Progression of Collagen Degeneration of Cartilage in the Knee: Data from the Osteoarthritis Initiative. Sci. Rep. 6:21415.

20. Venäläinen MS, Mononen ME, Väänänen SP, et al. 2016. Effect of bone inhomogeneity on

tibiofemoral contact mechanics during physiological loading. J. Biomech. 49(7):1111–1120.

21. Tanska P, Julkunen P, Korhonen RK. 2017. A computational algorithm to simulate disorganization of collagen network in injured articular cartilage. Biomech. Model. Mechanobiol. 17(3):689–699.

22. Kiapour A, Kiapour AM, Kaul V, et al. 2013. Finite Element Model of the Knee for Investigation of Injury Mechanisms: Development and Validation. J. Biomech. Eng. 136(1):011002.

23. Bartell LR, Fortier LA, Bonassar LJ, Cohen I. 2018. Measuring microscale strain fields in articular cartilage during rapid impact reveals thresholds for chondrocyte death and a protective role for the superficial layer. J. Biomech. 48(12):3440–3446.

24. Párraga Quiroga JM, Wilson W, Ito K, van Donkelaar CC. 2017. The effect of loading rate on the development of early damage in articular cartilage. Biomech. Model. Mechanobiol. 16(1):263–273.

25. Hosseini SM, Wilson W, Ito K, van Donkelaar CC. 2018. A numerical model to study mechanically induced initiation and progression of damage in articular cartilage. Osteoarthr. Cartil. 22(1):95–103.

26. Peña E, Calvo B, Martínez MA, Doblaré M. 2007. Effect of the size and location of osteochondral defects in degenerative arthritis. A finite element simulation. Comput. Biol. Med. 37(3):376–387.

27. Olson SA, Furman BD, Kraus VB, et al. 2015. Therapeutic opportunities to prevent post-traumatic arthritis: Lessons from the natural history of arthritis after articular fracture. J. Orthop. Res. 33(9):1266–1277.

28. D'Lima DD, Hashimoto S, Chen PC, et al. 2001. Cartilage Injury Induces Chondrocyte Apoptosis. J. Bone {&} Jt. Surg. 83(2 suppl 1).

29. Wilson W, van Burken C, van Donkelaar C, et al. 2006. Causes of mechanically induced collagen damage in articular cartilage. J. Orthop. Res. 24(2):220–228.

30. Sasazaki Y, Shore R, Seedhom BB. 2006. Deformation and failure of cartilage in the tensile mode. J. Anat. 208(6):681–694.

31. Wilson W, van Donkelaar CC, van Rietbergen B, et al. 2004. Stresses in the local collagen network of articular cartilage: a poroviscoelastic fibril-reinforced finite element study. J. Biomech. 37(3):357–366.

32. Wilson W, van Donkelaar CC, van Rietbergen B, et al. 2005. Erratum to "Stresses in the local collagen network of articular cartilage: a poroviscoelastic fibril-reinforced finite element study" [Journal of Biomechanics 37 (2004) 357–366] and "A fibril-reinforced poroviscoelastic swelling model for articular cartil. J. Biomech. 38(10):2138–2140.

33. Goodwin DW, Wadghiri YZ, Zhu H, et al. 2004. Macroscopic Structure of Articular Cartilage of the Tibial Plateau: Influence of a Characteristic Matrix Architecture on MRI Appearance. Am. J. Roentgenol. 182(2):311–318.

34. Benninghoff A. 1925. Form und Bau der Gelenkknorpel in ihren Beziehungen zur Funktion - Zweiter Teil: Der Aufbau des Gelenkknorpels in seinen Beziehungen zur Funktion. Zeitschrift für Zellforsch. und Mikroskopische Anat. 2(5):783–862.

35. Petersen W, Tillmann B. 1998. Collagenous fibril texture of the human knee joint menisci. Anat. Embryol. (Berl). 197(4):317–324.

36. Halonen KS, Mononen ME, Jurvelin JS, et al. 2014. Deformation of articular cartilage during

static loading of a knee joint – Experimental and finite element analysis. J. Biomech. 47(10):2467–2474.

37. Villegas DF, Maes JA, Magee SD, Haut Donahue TL. 2007. Failure properties and strain distribution analysis of meniscal attachments. J. Biomech. 40(12):2655–2662.

38. Taddei F, Pancanti A, Viceconti M. 2004. An improved method for the automatic mapping of computed tomography numbers onto finite element models. Med. Eng. Phys. 26(1):61–69.

39. Taddei F, Schileo E, Helgason B, et al. 2007. The material mapping strategy influences the accuracy of CT-based finite element models of bones: An evaluation against experimental measurements. Med. Eng. Phys. 29(9):973–979.

40. Kutzner I, Heinlein B, Graichen F, et al. 2018. Loading of the knee joint during activities of daily living measured in vivo in five subjects. J. Biomech. 43(11):2164–2173.

41. Bergmann G, Bender A, Graich F, et al. 2014. Standardized Loads Acting in Knee Implants. PLoS One 9(1):1–12.

42. Mononen ME, Jurvelin JS, Korhonen RK. 2015. Implementation of a gait cycle loading into healthy and meniscectomised knee joint models with fibril-reinforced articular cartilage. Comput. Methods Biomech. Biomed. Engin. 18(2):141–152.

43. Kozanek M, Hosseini A, Liu F, et al. 2009. Tibiofemoral kinematics and condylar motion during the stance phase of gait. J. Biomech. 42(12):1877–1884.

44. Li J-S, Tsai T-Y, Wang S, et al. 2014. Prediction of In Vivo Knee Joint Kinematics Using a Combined Dual Fluoroscopy Imaging and Statistical Shape Modeling Technique. J. Biomech. Eng. 136(12):124503–124506.

45. Mow VC, Ratcliffe A, Robin Poole A. 1992. Cartilage and diarthrodial joints as paradigms

for hierarchical materials and structures. Biomaterials 13(2):67–97.

46. Federico S, Herzog W. 2008. On the anisotropy and inhomogeneity of permeability in articular cartilage. Biomech. Model. Mechanobiol. 7(5):367–378.

47. Wilson W, van Burken C, van Donkelaar CC, et al. 2006. Causes of mechanically induced collagen damage in articular cartilage. J. Orthop. Res. 24(2):220–228.

48. R Core Team. 2017. R Core Team. R: A language and environment for statistical computing. R Found. Stat. Comput. Vienna, Austria. URL http//www.R-project.org/.

49. Hunter DJ, Guermazi A, Lo GH, et al. 2011. Evolution of semi-quantitative whole joint assessment of knee OA: MOAKS (MRI Osteoarthritis Knee Score). Osteoarthr. Cartil. 19(8):990–1002.

50. Flanigan DC, Harris JD, Jia G, et al. 2014. Effect of Chondral Defect Size, Shape, and Location on MRI Diagnostic Performance in the Porcine Knee. Orthopedics 37(4):e322–e327.

51. Hjelle K, Solheim E, Strand T, et al. 2002. Articular cartilage defects in 1,000 knee arthroscopies. Arthrosc. J. Arthrosc. Relat. Surg. 18(7):730–734.

52. Dabiri Y, Li L. 2015. Focal cartilage defect compromises fluid-pressure dependent load support in the knee joint. Int. J. Numer. Method. Biomed. Eng. 31(6):e02713.

53. Heuijerjans A, Wilson W, Ito K, van Donkelaar CC. 2017. The critical size of focal articular cartilage defects is associated with strains in the collagen fibers. Clin. Biomech. 50:40–46.

54. Papaioannou G, Demetropoulos CK, King YH. 2010. Predicting the effects of knee focal articular surface injury with a patient-specific finite element model. Knee 17(1):61–68.

55. Gratz KR, Wong BL, Bae WC, Sah RL. 2009. The effects of focal articular defects on

cartilage contact mechanics. J. Orthop. Res. 27(5):584–592.

56. Fisher MB, Belkin NS, Milby AH, et al. 2015. Cartilage repair and subchondral bone remodeling in response to focal lesions in a mini-pig model: implications for tissue engineering. Tissue Eng. Part A 21(3–4):850–60.

57. Sharma L, Hochberg M, Nevitt M, et al. 2017. Knee tissue lesions and prediction of incident knee osteoarthritis over 7 years in a cohort of persons at higher risk. Osteoarthr. Cartil. 25(7):1068–1075.

58. Squires GR, Okouneff S, Ionescu M, Poole AR. 2003. The pathobiology of focal lesion development in aging human articular cartilage and molecular matrix changes characteristic of osteoarthritis. Arthritis Rheum. 48(5):1261–1270.

59. Guermazi A, Hayashi D, Roemer FW, et al. 2016. Partial- and Full-thickness focal cartilage defects equally contribute to development of new cartilage damage in knee osteoarthritis - the Multicenter Osteoarthritis Study. Arthritis Rheumatol. 69(3):560–564.

60. Orozco GA, Tanska P, Florea C, et al. 2018. A novel mechanobiological model can predict how physiologically relevant dynamic loading causes proteoglycan loss in mechanically injured articular cartilage. Sci. Rep. 8(1):15599.

61. Eskelinen ASA, Mononen ME, Venäläinen MS, et al. 2019 [Epub ahead of print]. Maximum shear strain-based algorithm can predict proteoglycan loss in damaged articular cartilage. Biomech. Model. Mechanobiol. doi: 10.1007/s10237-018-01113-1.

62. Goldring SR, Goldring MB. 2016. Changes in the osteochondral unit during osteoarthritis: structure, function and cartilage-bone crosstalk. Nat. Rev. Rheumatol. 12(11):632–644.

63. Mononen ME, Mikkola MT, Julkunen P, et al. 2012. Effect of superficial collagen patterns

and fibrillation of femoral articular cartilage on knee joint mechanics-A 3D finite element analysis. J. Biomech. 45(3):579–587.

64. Räsänen LP, Tanska P, Zbýň Š, et al. 2017. The effect of fixed charge density and cartilage swelling on mechanics of knee joint cartilage during simulated gait. J. Biomech. 61:34–44.

65. Mononen ME, Tanska P, Isaksson H, Korhonen RK. 2018. New algorithm for simulation of proteoglycan loss and collagen degeneration in the knee joint: Data from the osteoarthritis initiative. J. Orthop. Res. 36(6):1673–1683.

66. Räsänen LP, Mononen ME, Lammentausta E, et al. 2016. Three dimensional patient-specific collagen architecture modulates cartilage responses in the knee joint during gait. Comput. Methods Biomech. Biomed. Engin. 19(11):1225–1240.

67. Räsänen LP, Tanska P, Mononen ME, et al. 2016. Spatial variation of fixed charge density in knee joint cartilage from sodium MRI – Implication on knee joint mechanics under static loading. J. Biomech. 49(14):3387–3396.

68. van Tiel J, Siebelt M, Waarsing JH, et al. 2012. CT arthrography of the human knee to measure cartilage quality with low radiation dose. Osteoarthr. Cartil. 20(7):678–685.

69. Mittelstaedt D, Xia Y. 2015. Depth-Dependent Glycosaminoglycan Concentration in Articular Cartilage by Quantitative Contrast-Enhanced Micro-Computed Tomography. Cartilage 6(4):216–225.

70. Lakin BA, Ellis DJ, Shelofsky JS, et al. 2015. Contrast-enhanced CT facilitates rapid, non-destructive assessment of cartilage and bone properties of the human metacarpal. Osteoarthr. Cartil. 23(12):2158–2166.

71. Liukkonen MK, Mononen ME, Klets O, et al. 2017. Simulation of Subject-Specific

Progression of Knee Osteoarthritis and Comparison to Experimental Follow-up Data: Data from the Osteoarthritis Initiative. Sci. Rep. 7(1):9177.

72. Gilbert S, Chen T, Hutchinson ID, et al. 2014. Dynamic contact mechanics on the tibial plateau of the human knee during activities of daily living. J. Biomech. 47(9):2006–2012.

73. Poh S-Y, Yew K-SA, Wong P-LK, et al. 2012. Role of the anterior intermeniscal ligament in tibiofemoral contact mechanics during axial joint loading. Knee 19(2):135–139.

74. Thambyah A, Goh JCH, De S Das. 2005. Contact stresses in the knee joint in deep flexion. Med. Eng. Phys. 27(4):329–335.

75. Bolcos PO, Mononen ME, Mohammadi A, et al. 2018. Comparison between kinetic and kinetic-kinematic driven knee joint finite element models. Sci. Rep. 8(1):17351.

76. Adouni M, Shirazi-Adl A. 2014. Evaluation of knee joint muscle forces and tissue stresses-strains during gait in severe OA versus normal subjects. J. Orthop. Res. 32(1):69–78.

77. Hosseini A, Van de Velde SK, Kozanek M, et al. 2010. In-vivo time-dependent articular cartilage contact behavior of the tibiofemoral joint. Osteoarthr. Cartil. 18(7):909–916.

Figure legends

Figure 1. a) Global model of the knee was constructed based on the 3D geometries generated from the arthrographic CT image segmentations. The collagen architecture in the cartilage and bone mineral density were taken into account in the model, similarly as in previous studies[18,20]. In all cases, physically relevant loading, mimicking the stance phase of gait, was used to simulate joint function[40,41]. **b)** For all lesion sites, submodels with substantially denser meshes (average element edge length ~0.7mm) were created to obtain even more accurate estimation of strains in tissue surrounding the lesion. **c)** All analyses were carried out using values obtained from the detailed strain distributions. In the given example, a noticeable elevation in maximum principal (tensile) strains can be observed (red) in the edges of the lesion.

Figure 2. a) Locations and shapes of the lesions located at the medial femoral condyle (n = 5). Each row in the figure represents one lesion site. The red dashed line on top of the lesion geometry represents the location of the crosscut slices. Maximum principal (tensile) strain distributions differed noticeably between the models with **b)** intact and **c)** defected cartilage. The time points selected for each comparison of intact and defected cartilage comparison correspond to the phase of stance with maximum difference in peak values between the models.

Figure 3. a) Locations and shapes of the lesions at the lateral femoral condyle (n = 2, top of the figure) and tibial condyle (n = 2, bottom of the figure) modeled in this study. Each row at the figure represents one lesion site. The red dashed line on top of the lesion geometry represents the location of the crosscut slices. Maximum principal (tensile) strain distributions differed between the models with **b)** intact and **c)** defected cartilage. The time points selected for each intact versus defected cartilage comparison correspond to the phase of stance when maximum difference in peak values between the models was observed.

Figure 4. Peak values of maximum principal strains, minimum principal strains, and maximum shear strains in tissue surrounding the lesion (within 1 mm distance) for models with defected and intact

cartilage during the entire stance phase of gait. The red horizontal lines in the images represents the suggested failure limit of cartilage tissue based on the literature[28,47]. Based on this, the lesions can be separated into higher risk and lower risk groups.

Figure 5. Illustration of the cumulative stress levels of the lesions. Each value is normalized to the maximum cumulative stress value at the current anatomical location of the lesion, for instance tibial condyle. Only two of the lesions are located at lower stress level region in the knee. Three radiuses represent normalized cumulative stress levels of 0, 0.5, and 0.9.

Table 1. Spearman correlation coefficients between lesion parameters (* $p < 0.05$, ** $p < 0.01$).

	Defect area	Defect volume	Defect cumulative stress	Change in max. prin. strain	Change in min. prin. strain	Change in max. shear strain
Defect max. depth	-	-	0.833**	0.767*	-0.400	0.917**
Defect area	-	-	0.900**	0.650	-0.333	0.750*
Defect volume		-	0.933**	0.717*	-0.467	0.733*
Change in max. principal strain				-	-0.800*	0.717*
Change in min. principal strain					-	-0.450

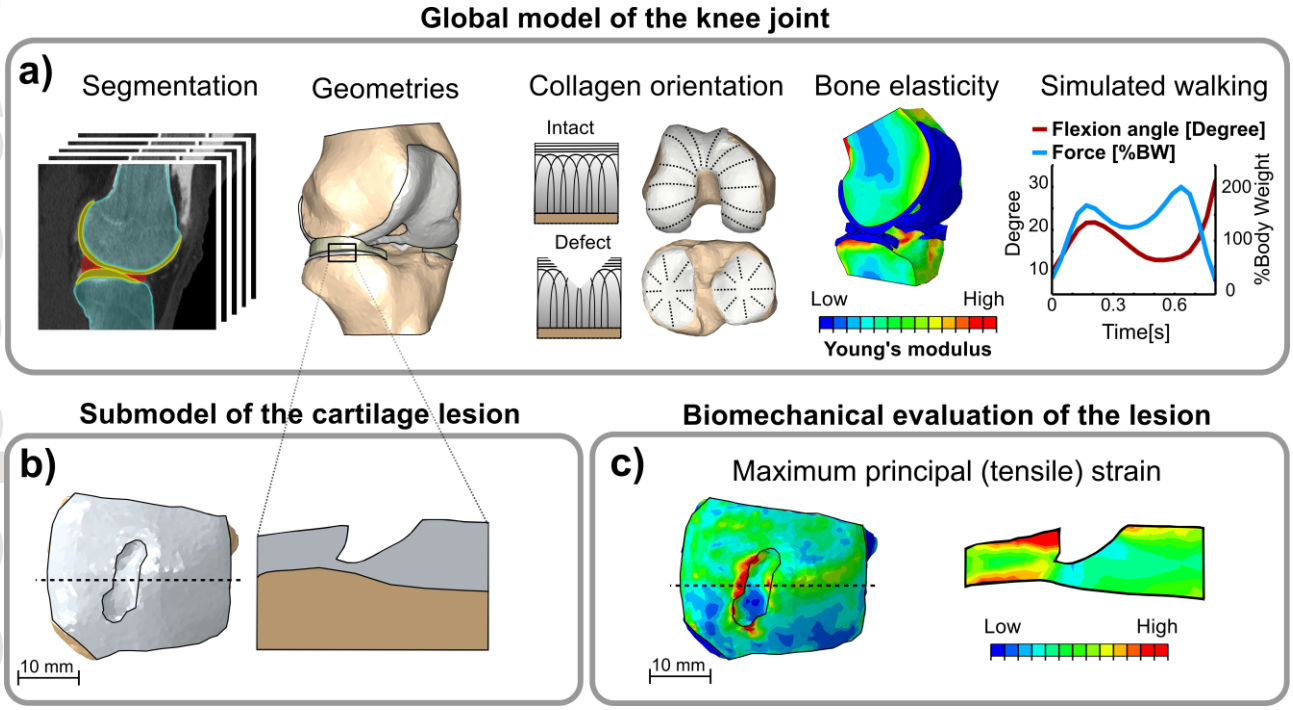

Figure 1

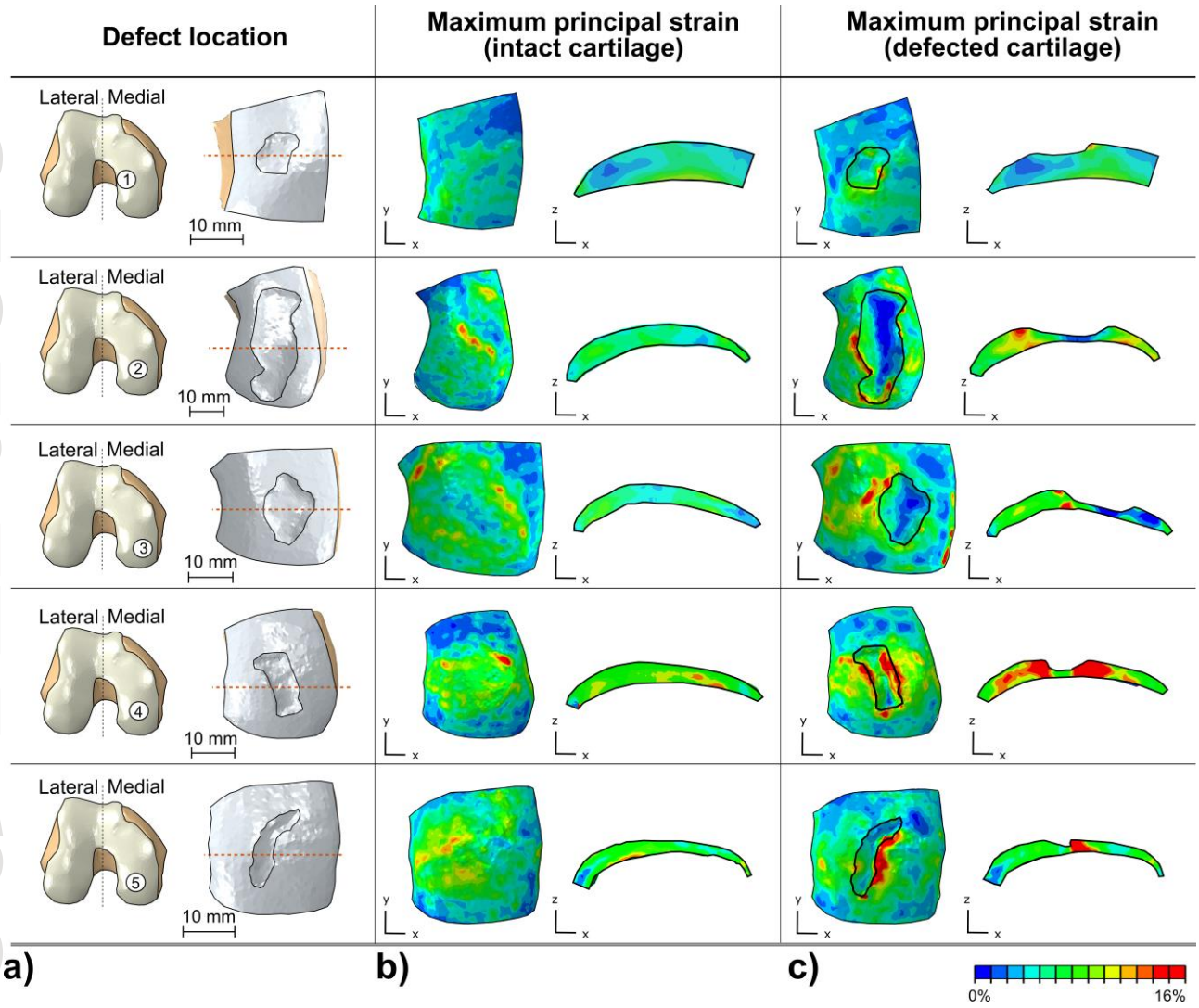

Figure 2

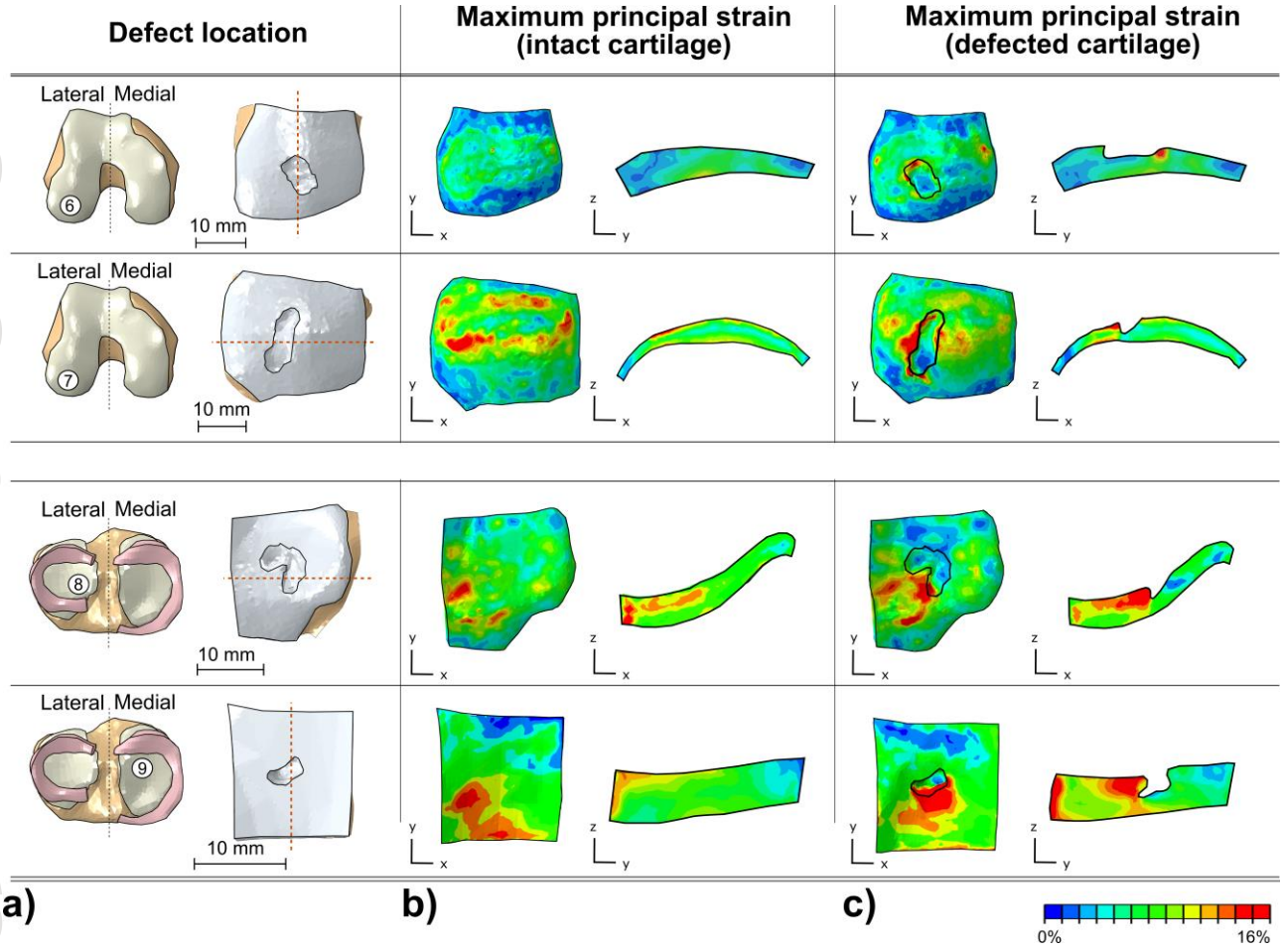

Figure 3

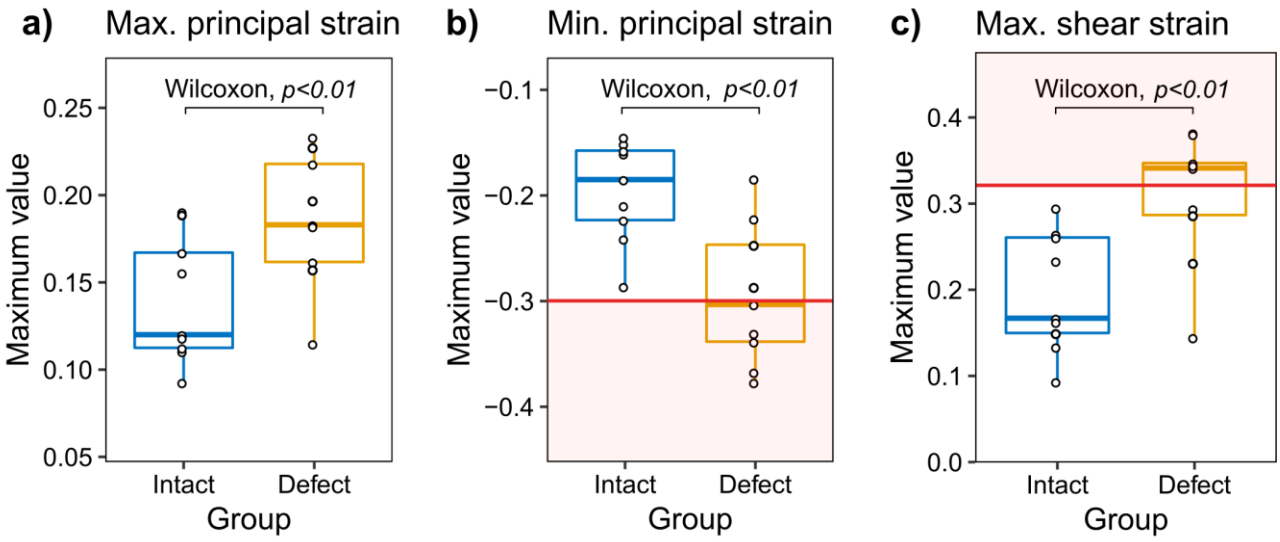

Figure 4

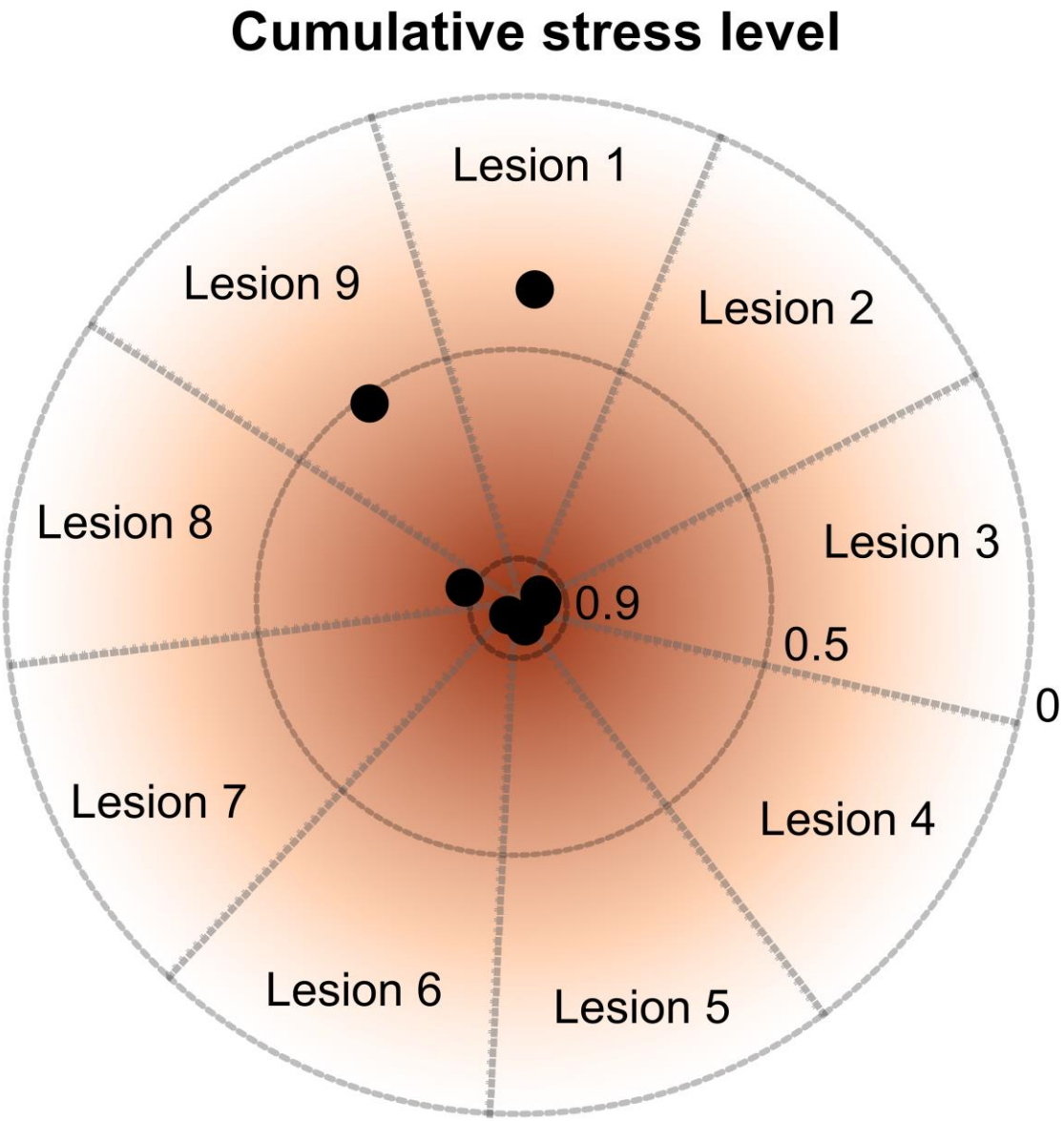

Figure 5